

A FOUNDRY FABRICATED HIGH-SPEED ROTATION SENSOR USING OFF-CHIP RF WIRELESS SIGNAL TRANSMISSION

Winston Sun¹, Antony W.-T. Ho¹, Wen J. Li^{*1}, John D. Mai², and Tao Mei³

¹*Department of Mechanical and Automation Engineering, The Chinese University of Hong Kong, Hong Kong SAR*

²*Department of Mechanical and Aerospace Engineering, University of California, Los Angeles, USA*

³*Institute of Intelligent Machines, Chinese Academy of Sciences, Hefei, Anhui, China*

ABSTRACT

A novel MEMS surface-micromachined non-contact high-speed rotation sensor with total surface area under 4mm² was developed using the MCNC Multi-User MEMS Processes (MUMPs). This paper reports the initial characterization of the sensor, including rotation and vibration tests. Initial results indicate that this piezoresistive sensor is capable of wirelessly measuring rotation speeds at ~2Hz/rpm/V with 5V input in the 100 to 6000rpm rotation range. We believe our groundwork will allow the MEMS community to use the MUMPs foundry service to design simple and reliable high-speed rotation sensors that can be interfaced with commercial wireless chips for signal transmission.

Key words: non-contact rotation sensing, high-speed rotation sensing, micro rotation sensor, wireless sensor.

INTRODUCTION

Tachometers have been widely used to measure the angular speeds of rotating objects. In general, contact mechanical-based tachometers, although capable of giving measurements conveniently, are less accurate than AC or DC electromagnetic-based tachometers. Nevertheless, each type has its own advantages and shortcomings depending on the applications [1,2]. Optical tachometers are also available that give relatively accurate readings with wide rpm range [3,4]. However, Kwa et al. [5] pointed out that some optical sensors are quite sensitive to background light and contamination.

Recently, many new sensor devices based on different principles, including non-contact magnetic field [6], Faraday induction [7], and capacitive [8], have been built. These techniques, however, impose restrictions on the material properties or geometry of the rotational components to be measured, and they also limit the effective measurable rotation speed. In addition, all these sensors must be accompanied with a stationary reference, which is externally mounted to the systems' housing for proper operation.

We propose to build a MEMS rotation sensor with no external reference sensor that can be potentially integrated with wireless-transmission electrical circuitry. Since these micromachined sensors will be

small, they can be directly embedded into the rotating objects such as gears or shafts. Many MEMS motion sensors have been fabricated using piezoelectric, piezoresistive, or capacitive principles [9,10,11]. However, the existing sensors are designed mainly for low angular speeds (i. e., <1000rpm) and acceleration measurements. In addition, to the best of our knowledge, no high-speed rotation sensors were built using the MCNC commercial foundry service and have wireless transmitted output.

This paper presents the design, analysis, and initial experimental results of polysilicon cantilever beam rotation sensors that can measure angular speeds between 100 to 6000rpm. These sensors are designed to have small size, low power consumption, low cost, wide dynamic range, and yet accurate. For demonstration, we have selected to use the MCNC MUMPs foundry to fabricate the mechanical elements that were then interfaced with commercial wireless transmission chips.

SENSOR CONCEPT AND DESIGN

The concept for measuring rotation of a spinning body using embedded micro-sensors is illustrated in Figure 1. A three dimensional illustration of a sensor is shown in Figure 2. We have used the MCNC MUMPs process to fabricate the sensor shown in this figure. The oxide layer underneath the mass platform was sacrificially released using hydrofluoric acid and critical CO₂ drying process. Etch holes were needed to provide shorter release etch paths under large features such as the mass platform, which is supported only by two polysilicon cantilever beams and therefore is free for deflection by centrifugal force. Scanning electron microscope (SEM) picture of a pair of the surface-micromachine sensors is shown in Figure 3. The mass platforms are sacrificially released and are curved due to residual stresses between different thin film layers in this case. Three MUMPs thin film layers which make up the platforms are apparent in this picture: Poly 1, Poly 2, and Au. A reference sensor structure that was not sacrificially released is shown in Figure 4. An interferometric image showing the curvature of a sacrificially released mass platform in both transverse and axial directions is shown in Figure 5.

* Corresponding Author: *The Chinese University of Hong Kong, Department of Mechanical and Automation Engineering, MMW 425, Shatin, NT, Hong Kong. Email: wen@mae.cuhk.edu.hk.*

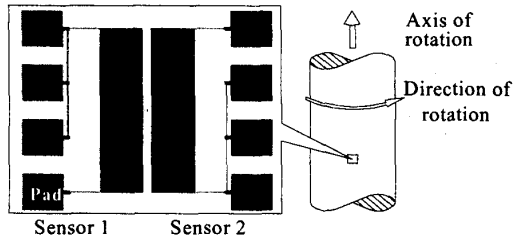


Figure 1. Conceptual drawing of micro-sensors embedded in rotating structures to measure rotation (not to scale).

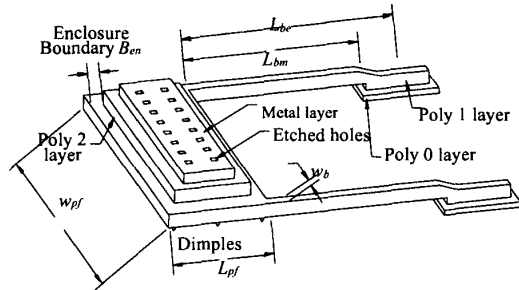


Figure 2. Three dimensional drawing of a surface-micromachined rotation sensor using polysilicon as cantilever beams supporting a multi-layered mass platform.

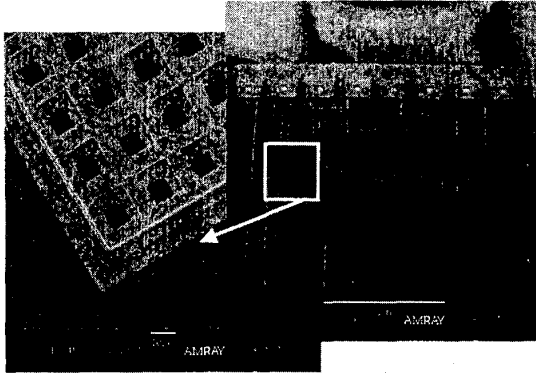


Figure 3. SEM picture of a pair of fabricated sensors. The curvature of the mass plate is due to residual stress between different layers of materials making up the plate.

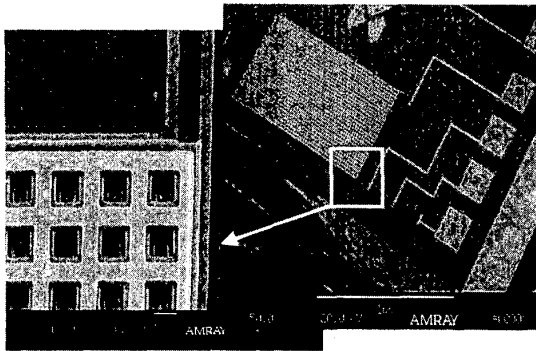


Figure 4. SEM picture of a reference sensor. MUMPs layers shown in the SEM include Poly 0, Poly 1, Poly 2, and Au.

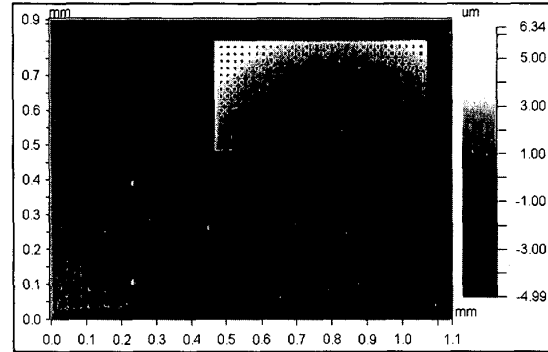


Figure 5. Interferometric image of a surface micro-machined rotations sensor.

Theoretical Analysis

As shown in Figure 6, a set containing two identical sensors in opposite directions is oriented so that the axes of the cantilevered beams are perpendicular to the axis of rotation. As will be discussed later, a set of 2 sensors can be used to measure the angular acceleration of the rotating element. If no linear motion exists along the rotation axis then lateral deflection of the beams, or transverse stress, can be neglected. Excluding the substrate, a MCNC fabricated sensor is less than $5.1\mu\text{m}$ thick (platform) and weighs about 3 to $15\mu\text{g}$, depending on the platform size. As shown in Figure 6, the initial moment arm from the centroid c to the fixed end F is a constant. When a centrifugal force is induced on the seismic mass by an angular velocity (ω) or acceleration (α), the length of this moment arm will change. Also, the transverse load $P = m \cdot r \cdot \omega^2$ induced by rotation and the axial load $N = m \cdot r \cdot \alpha$ caused by angular acceleration (r is the distance from the axis of rotation to the neutral axis of the cantilever) both act on the centroid c of the platform. The distance e_c is a constant depending on the number of polysilicon layers. It is measured from the centroid of the platform to the neutral axis of the beam. The maximum strain on the cantilever beams occurs at F , the fixed end of the beams. From Fan et al. [12] the maximum allowable strain of polysilicon is about 1.7%. At $t > 0$ sec, the platform will be raised by a distance h_{cg} due to centrifugal force. Consequently the beams will be under stress and deformed in a curved shape. The beams will also undergo slight elongation or shortening depending on the combined effect of P and N . The moment arm measured from the fixed end F to the centroid will also be shifted from initial distance to arm_{cg} .

The governing differential equation for the bending beam is shown in Equation 1 below. The moment and stress equations are shown in Equations 2 and 3, respectively.

$$EI \frac{d^2 y_i}{dx_i^2} + P \cdot x \pm N \cdot y - M_i = 0 \quad (1)$$

$$M_i = P \cdot arm_{cg} \pm N \cdot h_{cg} \quad (2)$$

$$\sigma_i = M_i \cdot (t_{bm}/2)/I_{bm} \mp N/A_{bm}, i = 1, 2 \quad (3)$$

The index i denotes sensors 1 and 2 in Figure 6. In Equation 3 I_{bm} is the moment of inertia of the cross-section area about the neutral axis. $A_{bm} = t_{bm}(2 \cdot w_{bm})$ is the total cross-section area of the two beams. Equation 2 is obtained by summing the moments about any arbitrary point (x, y) along the beam i . Analytical solutions of Equation 1 can be readily obtained from symbolic mathematical packages (i.e., Mathematica) for a given set of values of r , ω and α . For transient calculations, the results of Equation 1 can be used to obtain arm_{cg} and h_{cg} at a given time, which can then be used in Equation 2 to obtain a more accurate solution.

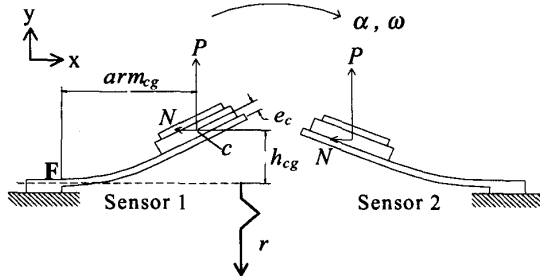


Figure 6. This illustration shows a pair of rotation sensors. The design parameters are also shown in this figure.

The deflection or elongation of the beams causes a change of resistance of the polysilicon, which can be converted into a measurable change of voltage by connecting the sensors in a Wheatstone-bridge configuration [12]. The change of resistance due to beam elongation can be expressed as a function of gauge factor G or in terms of the piezoresistance coefficient π_{44} [14]. This is shown in Equation 4:

$$\frac{\Delta R_i}{R} = \frac{G}{L_{bm}} \cdot \int_0^{L_{bm}} \frac{\sigma_i}{E} dx = \frac{\pi_{44}}{2} \cdot (\sigma_{li} - \sigma_{ti}) \quad (4)$$

where R is the total resistance of the sensor and for polysilicon is typically about $10 \Omega/\text{sq}$. [15]. π_{44} is taken to be $138.1 \times 10^{-11} \text{ Pa}^{-1}$, a result published by Smith [16] and verified by Beaty et al. [17]. σ_i is the longitudinal stress in Equation 3, and σ_t is the transverse stress which can be neglected at steady state conditions. When a steady state rotational speed is achieved, axial load N tends to zero. The two sensors

will have the same deflection and change of resistance. However, when the angular acceleration α is $\gg 0$, such as during motor startup or under sudden change of speed, the transient response of Sensor 1 and Sensor 2 will be different due to the contribution from N . Hence, by monitoring the transient response of the sensors, the direction of acceleration can be determined. We have used the above theoretical analysis in designing the sensors to measure angular speeds up to 8000rpm.

EXPERIMENTAL RESULTS

Each MCNC run gave us 15 chips that have 10 rotation sensors and other devices designed for our various on-going projects. We have measured the change of resistance due to bending of the piezoresistive polysilicon cantilever beams for sensors of different designed parameters on different MCNC chips. Table 1 is a representative comparison of sensor designs with different cantilever beam widths (W), lengths (L), and platform sizes. In the table, f denotes failure of the beams due to excessive strain at the given deflection angle. The deflection angle is the angle between the tip of the mass platform and the substrate. The resistance change typically varies from 0.5 to 2% as shown in the table.

Wireless Transmission Chips

Commercial wireless transmitters and receivers which can be eventually interfaced with the MEMS sensors were evaluated for signal transmission. Two basic configurations were evaluated. The first configuration, as shown in Figure 7, maps the analog voltage output from the sensor into digital data before RF transmission of the data by the transmitter. The volume of the entire transmitter circuitry, including the sensor, battery, and IC chip packaged ADC, clock, and RF transmitter is about $1\text{cm} \times 3\text{cm} \times 3\text{cm}$. When the ADC, clock, and RF transmitter die are used instead of the IC packaged chips the entire transmitter circuitry should be significantly smaller. A second type of transmission scheme, which maps the voltage from a sensor into frequency before the RF transmission, is shown in Figure 8. The overall volume of the IC packaged chips for this scheme is only 1/3 the size of the previous method but a frequency counter must be used at the receiver end to decipher the original voltage information.

platform size: 600x320					platform size: 600x1200						
defl. angle	W=30 μm , R_{30} : 154.9 Ω		W=14 μm , R_{14} : 266.75 Ω		defl. angle	W=20 μm , R_{20} : 223.15 Ω		W=30 μm , R_{30} : 146.64 Ω		L=200 μm , W=20 μm , R_{20} : 369.05 Ω	
	ΔR_i (Ohms)	%	ΔR_i (Ohms)	%		ΔR_i (Ohms)	%	ΔR_i (Ohms)	%	ΔR_i (Ohms)	%
25	0.474	0.306	1.364	0.511	25	0.866	0.388	0.489	0.333	0.765	0.207
35	0.852	0.550	2.687	1.007	35	1.566	0.702	0.778	0.531	1.190	0.322
45	1.292	0.834	3.963	1.486	45	2.407	1.079	1.157	0.789	1.843	0.499
55	f	f	5.486	2.057	55	3.467	1.554	1.620	1.105	2.518	0.682

Table 1. Deflection of the platform varies with cantilever beam dimensions. "Relative deflection" is difference between the lowest and highest points in the longitudinal or lateral dimensions of the platform.

We have adopted the second configuration at this time because it is simpler to build and has a good transmission performance experimentally. However, we have found that the TX2 transmitter (Radiometrix) works better than the HX2000 (RFM) for our sensors. The configuration is implemented as shown in Figure 9. The change of resistance across the bending beams (ΔR_3) is transduced into a change of differential voltage and then amplified by the AMP04 instrumentation amplifier, which has an adjustable gain between 1 and 1000. The amplified voltage is then converted into frequency signal by an AD654 voltage to frequency converter. This stage is essential for the TX2 transmitter to provide stable signal transmission. The potentiometer at R_4 should be adjusted such that variation of bridge output is beyond the initial offset and within the linear region of AD620 as well as bounded by the upper frequency limit of TX2 at around 28 kHz. The signal is detected wirelessly by the Radiometrix RX2 (not shown in the figure).

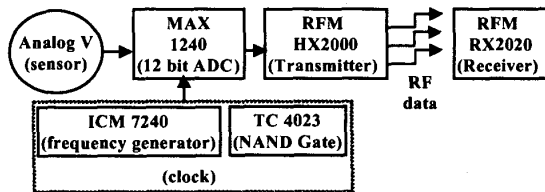


Figure 7. Block diagram for digital transmission of sensor data. Sensor data is digitized before RF transmission.

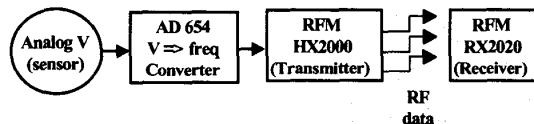


Figure 8. Block diagram for digital transmission of sensor data where the sensor data is mapped to a frequency domain before transmission.

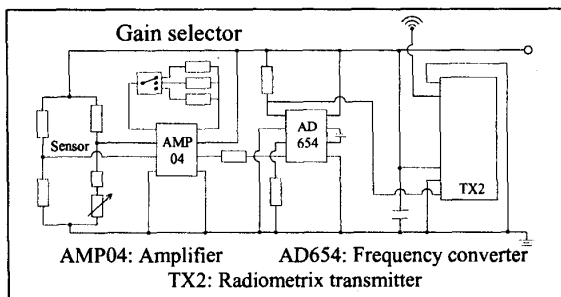


Figure 9. Schematic drawing of the wireless transmission circuit system which is used to transmit the surface-micromachined sensor.

Experimental Setup

Figure 10 is a conceptual drawing of the test setup for measuring the rotation speed of a disk wirelessly using the fabricated sensors. In our design the rotating disk is replaceable. The power supply, and the wireless data transmission chips are placed within a small package

made by a CNC plastic injection machine, which is then placed on the rotating disk. An illustration and a picture of the actual experimental apparatus is shown in Figure 10.

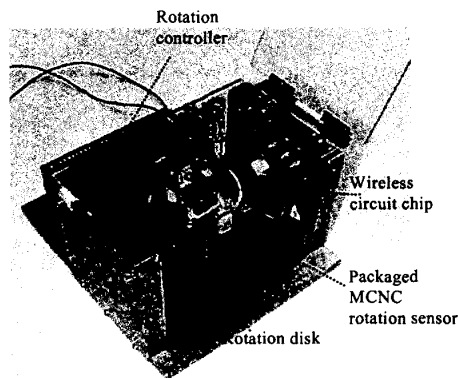
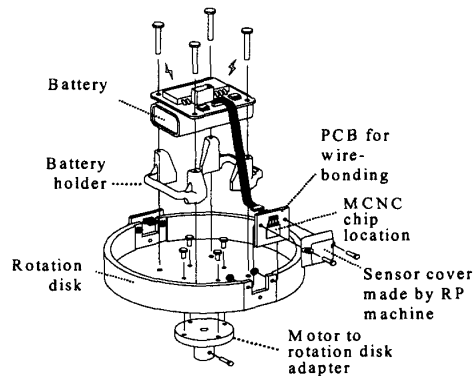


Figure 10. Conceptual drawing and actual picture of the experimental rotating disk packaged with wireless rotation MEMS sensors.

Sensor Results

The MCNC fabricated sensors were tested for piezoresistivity by using probes to lift the platforms while measuring changes in resistance across the beam-platform-beam connection (see Figure 1). The variations of resistance versus deflection angle of the platform from the substrate for several sensor designs are shown in Figure 11. Although the variations are non-linear they are very consistent. As predicted by theory, narrower beams give higher resistance change are prone to structural failure at higher deflection angles. For instance, $14 \times 100 \mu\text{m}$ beams will fail at $\sim 60^\circ$ while 20×200 and $30 \times 200 \mu\text{m}$ beams will survive beyond deflections angles of $\sim 80^\circ$ as shown in Figure 11.

The circuit shown in Figure 9 was calibrated using a potentiometer that has a nominal value close to R_3 (resistance of a designed sensor). The frequency output of the AD654 versus the change of the potentiometer (R_4) is linear over $\sim 20\%$ change of resistance (which gives a linear output frequency between 10 to 25 KHz). Each moving-platform sensor was connected to two

integrated polysilicon resistors on chip and a potentiometer off chip to form a Wheatstone bridge. The bridge output was connected via wirebonding to pads on a PCB that contains the signal transmission circuitry. Typical frequency output received by the RX2 receiver as the sensor is rotated is shown in Figure 12 and Figure 13. The response of the sensor, as shown in Figure 12, is non-linear as predicted, since the supporting cantilevered beams underwent large deflections over the dynamic range tested. The small-deflection beam theory does not hold for the entire sensor dynamic range, and hence, strains on the beams are not linearly proportional to the deflection. However, as indicated in Figure 13, for lower rotation speeds, the linear theory will hold, and the output of the bridge is proportional to V^2/R , where V is the tangential velocity of the rotating disk, and R the radius of the disk.

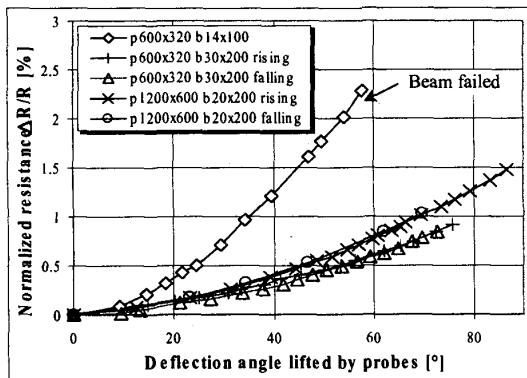


Figure 11. Change of resistance as a function of beam deflection.

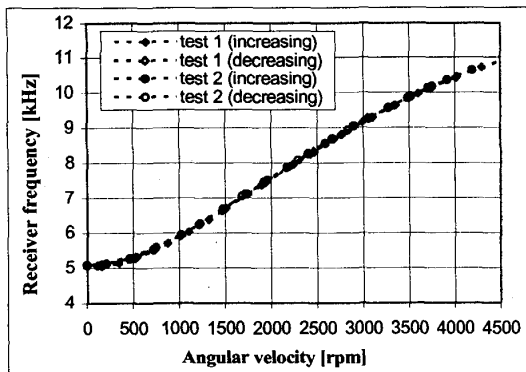


Figure 12. Wireless transmitted data from a rotation sensor. The sensor has a $1200 \times 600 \mu\text{m}^2$ platform supported by $20 \mu\text{m} \times 100 \mu\text{m}$ beams, and was rotated on a 10cm disk. Some sensors were tested up to 6000rpm before beam failure.

We have also developed an ANSYS model for the sensor structure to further investigate the non-linear effects of the bending cantilevers at high-speed rotations. The model will also allow us to predict sensor performance for more complex structural designs. Comparison of a ANSYS sensor-model result with the

theoretical results from equations 1 and 2 is shown in Figure 14. The results agree closely as shown, which, consequently, will allow us to 1) use the equations 1 and 2 to design and predict the performance of simple cantilever-platform sensors; 2) use ANSYS to determine the total piezoresistivity change of the sensor structure more accurately to include 3-dimensional effects on the strain of the sensor structure; 3) use ANSYS to design other sensor structures.

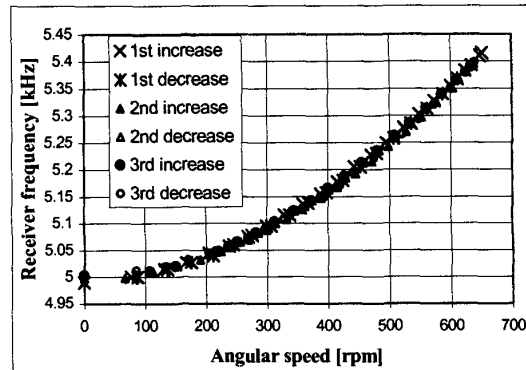


Figure 13. Wireless transmitted data from a sensor rotated at below 1000rpm (same sensor as Figure 10). Sensor response to angular rotation at lower speeds is different from at higher speeds.

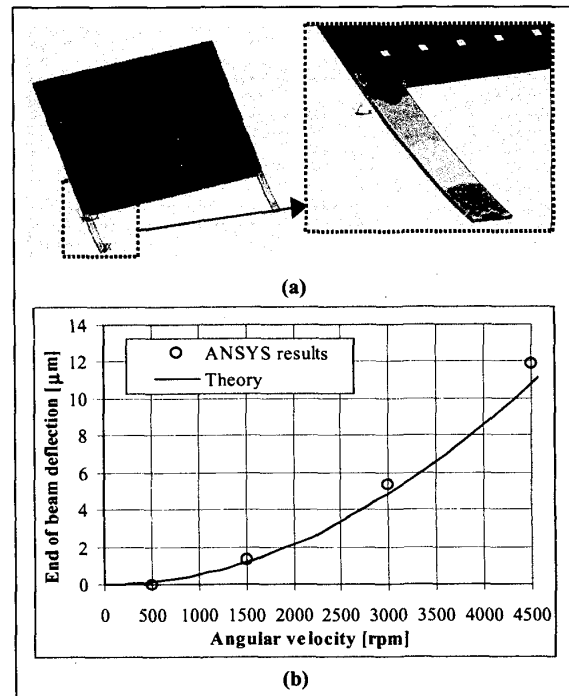


Figure 14. a) ANSYS model of a rotation sensor. b) Comparison of theoretical and ANSYS results for deflection of a sensor on a 10cm disk rotated up to 4500rpm. The structure analyzed has a $600 \times 320 \mu\text{m}^2$ platform with beam dimensions of $20 \mu\text{m} \times 100 \mu\text{m}$.

We have also attempted to predetermine the received frequency in the wireless transmission circuit versus the rotation speed using equations 1 to 4 (if the electronic gains are known a priori). However, equations 1 and 2 have assumed small and linear deflection in their formulation, hence can not predict the frequency output accurately for the entire experimental dynamic range, since the sensor structures will undergo large and non-linear deflections at high speeds. If Equation 4 is replaced with experimental data for resistance change versus deflection as given in Figure 11, then the prediction will be much more accurate. The comparison between the experimental results and aforementioned predictions is shown in Figure 15.

We have also subjected the sensors to the frequency and amplitude vibration range shown in Figure 16. The sensors have all survived vibrations both the longitudinal and lateral directions in the range given in the figure.

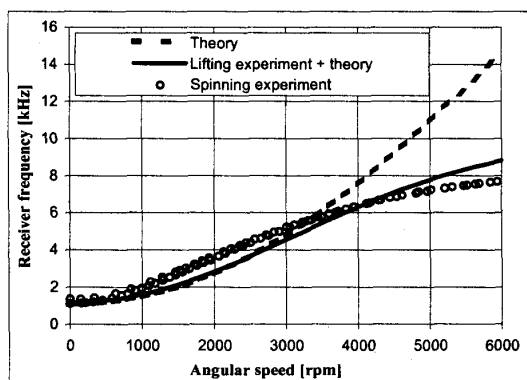


Figure 15. Comparison of experimental, theory, and theory plus lifting-experiment results. The theory under predicts sensor output possibly due to two factors: 1) piezoresistive change of the mass platform and 2) aerodynamic lifting of the mass platform.

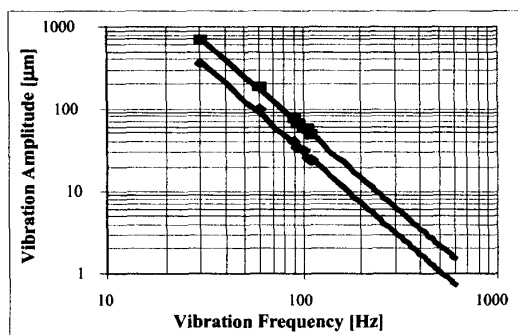


Figure 16. Amplitude versus frequency of the vibration used to test the sensors.

CONCLUSION

The design of a novel surface-micromachined rotation sensor is presented. It is designed to detect the angular velocity of a rotating element by measuring the resistance change due to stress induced by centrifugal

force on the seismic mass using piezoresistive effects. The designed sensors were fabricated using the MUMPS 29 run. Several wireless transmission schemes for the rotation sensors were evaluated and we have selected the Radiometrix transmission-receiving chips for our experiments. Experimental results showed a $13\mu\text{g}$ platform proof-mass could be used to detect rotation speeds of 100 to 6000rpm if appropriate structural designs are implemented. We will further improve the rotation sensing system by interfacing it with low-power wireless systems and also test the feasibility of using a pair of co-located structures for angular acceleration detection.

ACKNOWLEDGMENTS

We would like to thank Mr. Tin-Tak Tsang for contributing to the test and analysis of various commercial wireless transmission schemes. This work was funded by the Chinese University of Hong Kong Research Direct Grant.

REFERENCES

1. J. A. Haslam, et al., Engineering instrumentation and control, 1993, pp. 133.
2. C. L. Nachtigal, Instrumentation and control – Fundamentals and Applications, 1990, pp. 370.
3. <http://catalogue.pwallen.co.uk>.
4. R. C. Spooncer, et al., "An optical tachometer with optical fibre links", IEE Colloquium on IREM, 1991.
5. T. A. Kwa, et al., "An integrated high-resolution optical angular displacement sensor" IEEE Transducers '91, pp. 368-371.
6. K. Watanabe, et al., "Non-contact revolution measurement by the magnetic field intensity from axes", IEEE IMTC '94, 2, pp. 605-608.
7. A. Powell, et al., "Optimisation of magnetic speed sensors", IEEE Trans. on Mag. '96, 32, pp. 4977-9.
8. T. Fabian, et al., "A robust capacitive angular speed sensor", IEEE IMTC '97, 2, pp. 1267-1272.
9. J. Soderkvist, "Piezoelectric beams and angular rate sensors", IEEE Proc. on the 44th Annual Symposium On Frequency Control, 1990.
10. A. M. Madni, et al., "A microelectromechanical quartz rotational rate sensor for inertial applications", IEEE Aeros. App. Conf., 1996, 2, pp. 315-332.
11. R. Voss, et al., "Silicon angular rate sensor for automotive applications with piezoelectric drive and piezoresistive read-out", IEEE TRANSDUCERS '97, 2, pp. 879-882.
12. L. S. Fan, et al., IEEE Trans. on Electron Devices, 1988, 35, pp. 724-730.
13. T. G. Beckwith, et al., Mechanical measurements, 3rd edition, 1982.
14. B. Kloeck, "Piezoresistive sensors", Sensors – A comprehensive survey, 1994, 7, pp. 158-163.
15. D. A. Koester, et al., SmartMUMPS Design Handbook including MUMPs introduction and Design Rules Rev. 4.0, MEMS Technology Applications Center, March 1996.
16. C. S. Smith, Phys. Rev. 94, 1954, pp. 42-49.
17. R. E. Beaty, et al., "Evaluation of Piezoresistive coefficient variation in silicon stress sensors using a four-point bending test fixture", IEEE Trans. on CHMT '92, 15, pp. 904-914.